An Automated Method for Mapping Geomorphological Expressions of Former Subglacial Meltwater Pathways (Hummock Corridors) From High Resolution Digital Elevation Data

Emma L.M. Lewington[1], Stephen J. Livingstone[1], Andrew J. Sole[1], Chris D. Clark[1] and Felix S.L. Ng[1]

[1] Department of Geography, The University of Sheffield, Sheffield, S10 2TN.

Correspondence to Emma L.M. Lewington (elmlewington1@sheffield.ac.uk)

1. Introduction

Understanding the dynamic response of former (palaeo) continental ice sheets to climate change can provide valuable information for assessing the recent and predicting the future behaviour of the ice sheets in Antarctica and Greenland and their contribution to sea level rise (e.g. Ó Cofaigh and Stokes, 2008; Stokes et al., 2015 and references therein). Subglacially-produced landforms - exposed after glacial retreat - provide a rich record for reconstructing palaeo-ice sheets. Their distribution allows former ice sheet extent, relative thickness and retreat patterns to be reconstructed (e.g. Dyke & Prest, 1987; Boulton & Clark, 1990; Clark et al., 2004, 2012; Evans et al., 2005; Ottessen et al., 2008) and provides insight into ice sheet dynamics, thermal regime and subglacial hydrology (e.g. Kleman, 1992; Clark & Walder, 1994; Kleman & Borgstrom, 1996; Stokes & Clark, 1999; Kleman & Glasser, 2007; Margold et al., 2013, 2015; Storrar, et al., 2014; Livingstone et al., 2016).

Subglacial hydrological processes have been identified as a key factor of ice sheet dynamics (e.g. Iken, 1981; Boulton et al., 2001; Anderson et al., 2004; Schoof, 2010; Bartholomew et al., 2010). However, as the bed of contemporary ice sheets cannot be directly observed, the configuration of the subglacial drainage network is largely inferred from tracer and borehole monitoring studies and the use of ice dynamic proxies (e.g. Chandler et al., 2013; Andrews et al., 2014; Tedstone et al., 2015). In contrast, palaeo-ice-sheet-beds provide direct access to the landforms created by palaeo-subglacial meltwater drainage. These landforms can be used to determine the properties of the former subglacial drainage system at an ice sheet scale and throughout deglaciation, providing much needed context for spatially and

temporally limited contemporary observations. Subglacial meltwater landforms, such as meltwater channels, tunnel valleys and eskers, are widely observed in the geological record (e.g. Wright, 1973; Sharp et al., 1989; Clark and Walder, 1994; Greenwood et al., 2007; van der Vegt et al., 2012; Storrar et al., 2014; Livingstone and Clark, 2016) and have been routinely employed in glacial reconstructions to constrain former subglacial water flow direction, ice sheet surface slope and the position of the ice margin. The vastly improved resolution and coverage of digital elevation models (DEMs) today means that these landforms can be studied in greater detail and more comprehensively for such purpose. The associated datasets may thus also extend our understanding of some of the more complex processes related to subglacial meltwater flow (e.g. Makinen et al., 2017; Clark and Livingstone, 2018).

Here we focus on elongated tracts of hummocks that have been variously termed 'hummock corridors', 'glaciofluvial corridors' or 'subglacial meltwater corridors' (e.g. St-Onge, 1984; Rampton, 2000; Utting et al., 2009; Sharpe et al., 2017; Peterson and Johnson, 2018). Hummock corridors are believed to record former large-scale subglacial meltwater flow beneath ice sheets that is known to have been widespread, but whose origin is not yet fully understood (section 2). Given this uncertainty we use the non-genetic term 'hummock corridor' as per Peterson and Johnson (2018). Hummock corridors have been previously detected at a range of scales from field observations, aerial photographs, surficial geology maps and remotely sensed data (see references within Utting et al., (2009) and Sharpe et al., (2017) for a review of previous work in Canada and Peterson and Johnson (2018) for Sweden). The recent release of freely available high resolution DEMs (e.g.

ArcticDEM, Ladmateriat and Finland's National Land Survey) have vastly increased the evidence base of glacial features on palaeo-ice sheet beds. So widespread in fact, that the relatively slow process of manual mapping has become a major bottleneck for obtaining information about these features.

The objective of this paper is to demonstrate the utility of a new automatic method for mapping the large-scale distribution of hummock corridors from high-resolution DEMs to gain insight into their formation. The method is developed and tested on three test sites in northern Canada and northern Scandinavia. The success of the method was quantitatively determined by its ability to reproduce the large-scale distribution and morphometric characteristics (length and width) of the manually mapped hummock corridors.

2. Hummock Corridors

Hummock corridors have been identified and studied in detail in Canada (St-Onge, 1984; Rampton, 2000; Utting et al., 2009; Sharpe et al., 2017; Storrar and Livingstone, 2017) and Sweden (Peterson et al., 2017; Peterson and Johnson, 2018). They are defined as elongated tracts of irregular shaped hummocks which stand out from the surrounding smooth, streamlined bed (Fig. 1). Typical corridors are a few km to over 100 km long and 100s of m to several km wide (Table 1). The individual hummocks within the corridors vary in size (10s to 100s m in width/ length in plan view), shape (mostly irregular) and relief (1 to 10s of m) (Peterson and Johnson, 2018). In general, hummocks within the corridors tend to show no

consistent plan-form shape, although triangular-shaped hummocks have been identified in some corridors in Finland (Makinen et al., 2017) and Sweden (Peterson et al., 2017).

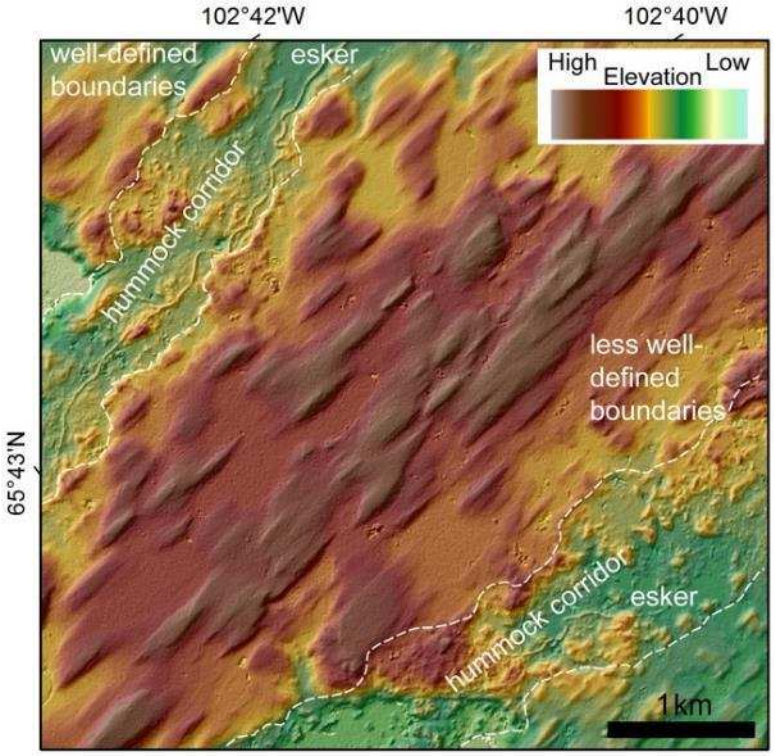

Figure 1. Hummock corridors in Keewatin, Nunavut, Canada (ArcticDEM). The corridors are aligned with and bordered by streamlined features on the bed that indicate ice-flow from the south to north.

Hummock corridors vary in topographic expression (Fig. 2); for example, adjacent corridors or different parts of the same corridor can be cut down into the surrounding former ice-sheet bed and/ or elevated above the surrounding terrain while other corridors branch and have tributaries. Some hummock corridors exhibit sharp boundaries with significant vertical relief, while other boundaries are more diffuse and characterised by subdued relief. Hummock corridors longitudinal elevation profiles are typically undulating and they often contain eskers. Although

tracts of hummocks can be traced over long distances (>100 km), they are often discontinuous with intervening segments of smoother terrain, tunnel valleys or eskers.

At a regional scale - i.e., a horizontal scale exceeding the size of individual corridors and approaching the size of the collection of multiple corridors and/ or the ice sheet - corridors appear to exhibit a radial pattern (e.g. Peterson and Johnson, 2018), indicative of a larger divergent network (Utting et al., 2009) and appear to be quasi-regularly spaced. Locally, corridors display a high degree of parallel conformity with each other and with other subglacial bedforms such as drumlins and lineations, suggesting a relationship with palaeo-ice flow.

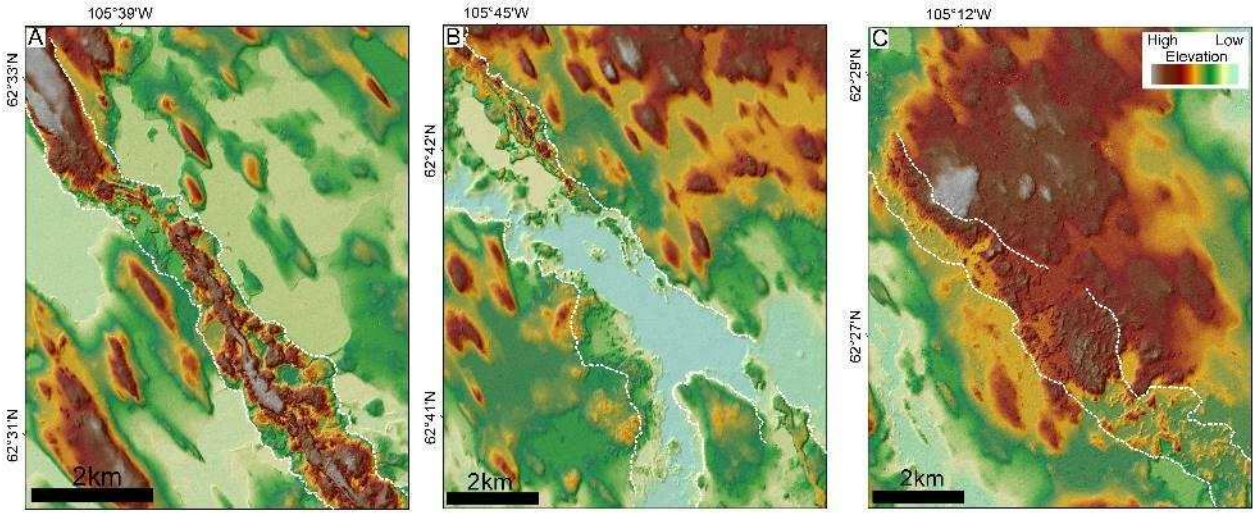

Figure 2. The variable expression of hummock corridors: (A) positive relief with a central esker (B) flat bedded sections and branching and (C) corridors without significant relief or eskers, identified simply as elongated tracts of hummocks. A-C are examples taken from within test site 1 (Fig. 9).

Adverse and undulating long profiles, orientations parallel to former glacier flow lines, the presence of eskers within the hummock corridors and the termination of corridors at or near former ice margins indicate a likely subglacial meltwater origin. However, the source of meltwater and the magnitude and duration of flow remains uncertain.

Table 1. Metrics of 'hummock corridor' type features reported in the literature.

Location	**Source**	**Term used**	**Frequency**	**Length (km)**	**Width (km)**	**Spacing (km)**
Southwestern Finland	Makinen et al. (2017)	Triangular-shaped landforms within distinguishable route	Single feature(s) selected for purpose	40 (longest feature)	1 – 2.5 (most distinct features)	1 – 4 (most distinct features)
Southern Swedish Uplands (SSU), Sweden	Peterson and Johnson (2018)	Hummock corridor	76 hummock tracts	1.5 – 11.8 (mean 5.2)	0.2 – 4.9 (mean 1.1)	0.8 – 54.5 (mean 14.5)
Southern Fraser Plateau, Canada	Burke et al. (2011)	Erosional corridor	Single	~ 40	~ 0.25 - 1	-
Southern Slave Province, Canada	Rampton (2000)	Meltwater corridor	-	-	0.5 - >2	-
East Arm Area, Great Slave Lake, Canada	Sharpe et al. (2017)	Meltwater erosional corridor	Approx. 22 corridors	80 - 120	~0.3 - 3	5 - 15
East-central Alberta and South-central Michigan	Sjogren et al. (2002)	Incipient tunnel channel	-	-	0.2 - 4	-
Redrock Lake Area, Canada	St-Onge (1984)	Glaciofluvial meltwater corridor	>15 (estimated from map)	Commonly > 20 (estimated from map)	Up to 1	12 – 15
Kivalliq region, Nunavut, Canada	Storrar and Livingstone (2017)	Corridor-like tracts of glaciofluvial deposits	-	-	Up to 6	-
Walker Lake, Canada	Utting et al. (2009)	Glaciofluvial corridor	>20 (estimated from map)	~ 5 - 12	~0.2 - ~ 0.7	5 – 10

Hummock corridors have similar widths, lengths and spacing as tunnel valleys (Table 1) which has led Peterson and Johnson (2018) to classify them as such. Proposed formation theories for the corridors thus far focus on similar concepts: (i) time-transgressive formation with small sections forming behind a retreating margin (St-Onge, 1984); (ii) low-frequency, high-magnitude regional outbursts with whole networks formed over relatively short periods (e.g. Rampton, 2000; Sharpe et al., 2017); or (iii) formation of individual channels by the sudden rapid drainage of large volumes of meltwater to the bed (e.g. Utting et al., 2009; Peterson and Johnson, 2018).

The formation of individual hummocks within the corridors has been ascribed to both deposition of glaciofluvial sediments within cavities during periods of sudden large meltwater influxes (e.g. Utting et al., 2009) and erosion by distributed braided canals on the bed of the valley or turbulent meltwater flow during valley formation (e.g. Sjogren et al., 2002; Peterson et al., 2018). Where the corridors and hummocks cut down into thicker till, formation is thought to be by subglacial fluvial erosion (Peterson and Johnson 2018), whereas positive relief corridors, or those containing tracts of glaciofluvial sands and gravels, have been associated with sediment deposition (e.g. Utting et al., 2009) and typically occur in areas where sediment thickness is low or the substrate is difficult to penetrate (Peterson and Johnson, 2017).

3. Methods

Traditionally, information on subglacial bedform distribution and morphology has been obtained by visual identification and onscreen digitization of feature boundaries (e.g. Clark et al., 2004; Greenwood and Clark, 2008; Hughes et al., 2010; Storrar et al., 2014; Livingstone and Clark, 2016). However, several issues are apparent with this approach, including the subjectivity of landform and boundary identification, concerns over which visualisation/ illumination techniques provide the best results (e.g. Smith and Clark, 2005; Hughes et al., 2010), and uncertainty regarding whether different practitioners produce the same consistent results (e.g. Hillier et al., 2015). Moreover, with the increasing availability and resolution of DEMs and remote sensing imagery, the immensity of data analysis required to manually explore and map large regions at such fine resolution is becoming a major bottleneck. Automatic or semi-automatic methods offer an alternative means of rapidly mapping and extracting quantitative information directly from DEMs (see Evans, 2012 and Bishop et al., 2012 for discussions).

Several studies have attempted to employ semi-automatic/ automatic techniques for mapping subglacial bedforms, particularly drumlins. These methods typically rely on an object based image analysis approach (OBIA) (e.g. Saha et al., 2011; Evans, 2012; Jorge and Brennand, 2017; Yu et al., 2015; Foroutan and Zimbelman, 2017), which uses a multi-resolution algorithm (Baatz and Schäpe, 2000) to group pixels into image objects and classify them based on predetermined rules (e.g. elevation, slope, axis, length, entropy and eccentricity).

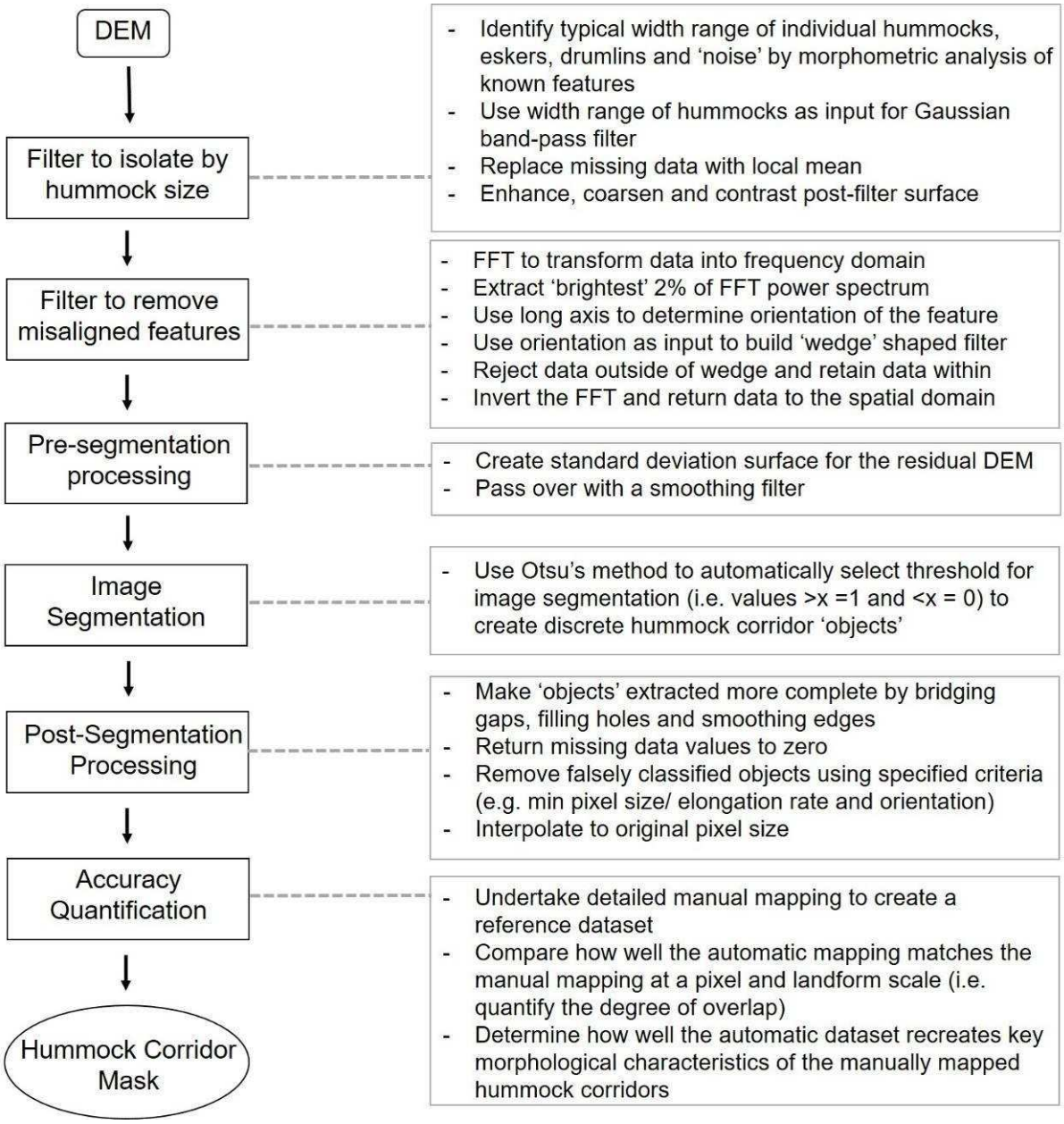

Figure 3. Main steps of our automatic method to identify and extract hummock corridors (left-hand sequence) with details about each step expanded on (right).

This study develops the first method to automatically map hummock corridors. Its main steps - detailed in Sections 3.1 to 3.4 - are outlined in Figure 3. The DEM tiles used come from the freely-available ArcticDEM dataset

(https://www.pgc.umn.edu/data/arcticdem), which provides 50 x 50 km tiles at 5 m resolution for all land area above 60°N. It was generated by applying stereo auto-correction techniques to overlapping pairs of high-resolution optical satellite images (Noh and Howat, 2015).

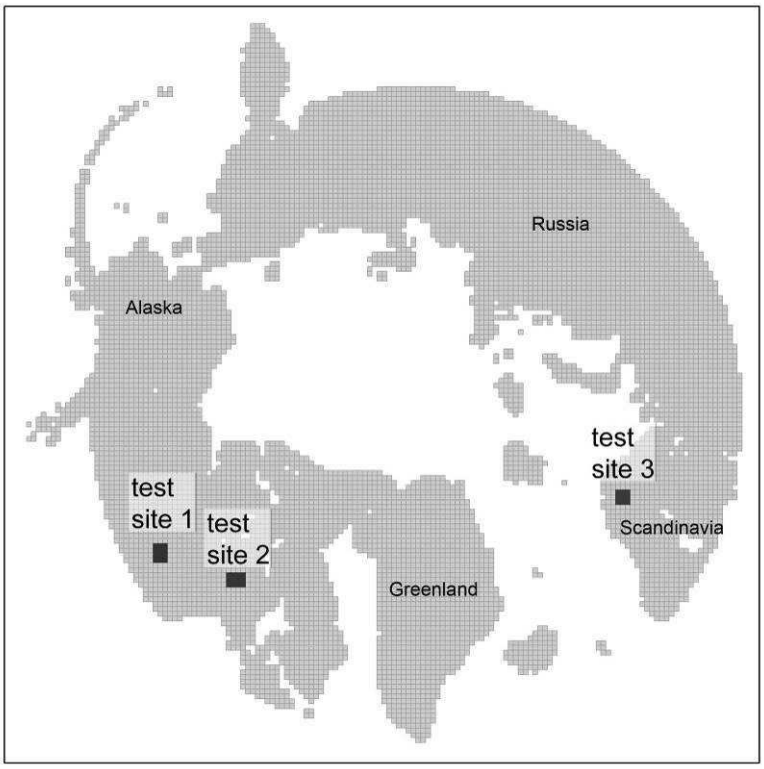

Figure 4. Location of the three test sites used in our study: (1) Northwest territories, Canada (30,000 km^2), (2) Nunavut, Canada (30,000 km^2) and (3) Northern Scandinavia (22,500 km^2). Grey background indicates the total extent of Arctic DEM data. See Fig. 5 for example of typical terrain from each test site.

To develop and test the automatic method, three test sites were selected from the ArcticDEM (Fig. 4), chosen to ensure a range of hummock corridor morphologies and background conditions were sampled (e.g. varying relief, presence/ absence of fluvial features etc.). At test site 1, corridors typically exhibit strong positive or

218 negative relief with well-defined edges, and are qualitatively clearly distinguished
219 from their surroundings (Fig. 5A). The site includes relatively straight hummock
220 corridors extending significant distances across the bed. At test site 2, the
221 background topography is more complex and hummock corridors tend to curve
222 across the landscape, exhibit less pronounced relief and have poorly defined
223 boundaries (Fig. 5B and C. The hummock corridors at test site 3 are typically
224 discontinuous and more subdued, and the surrounding landscape is characterised
225 by a strong fluvial network and significant vertical relief in the south-west of the site
226 (Fig. 5D).

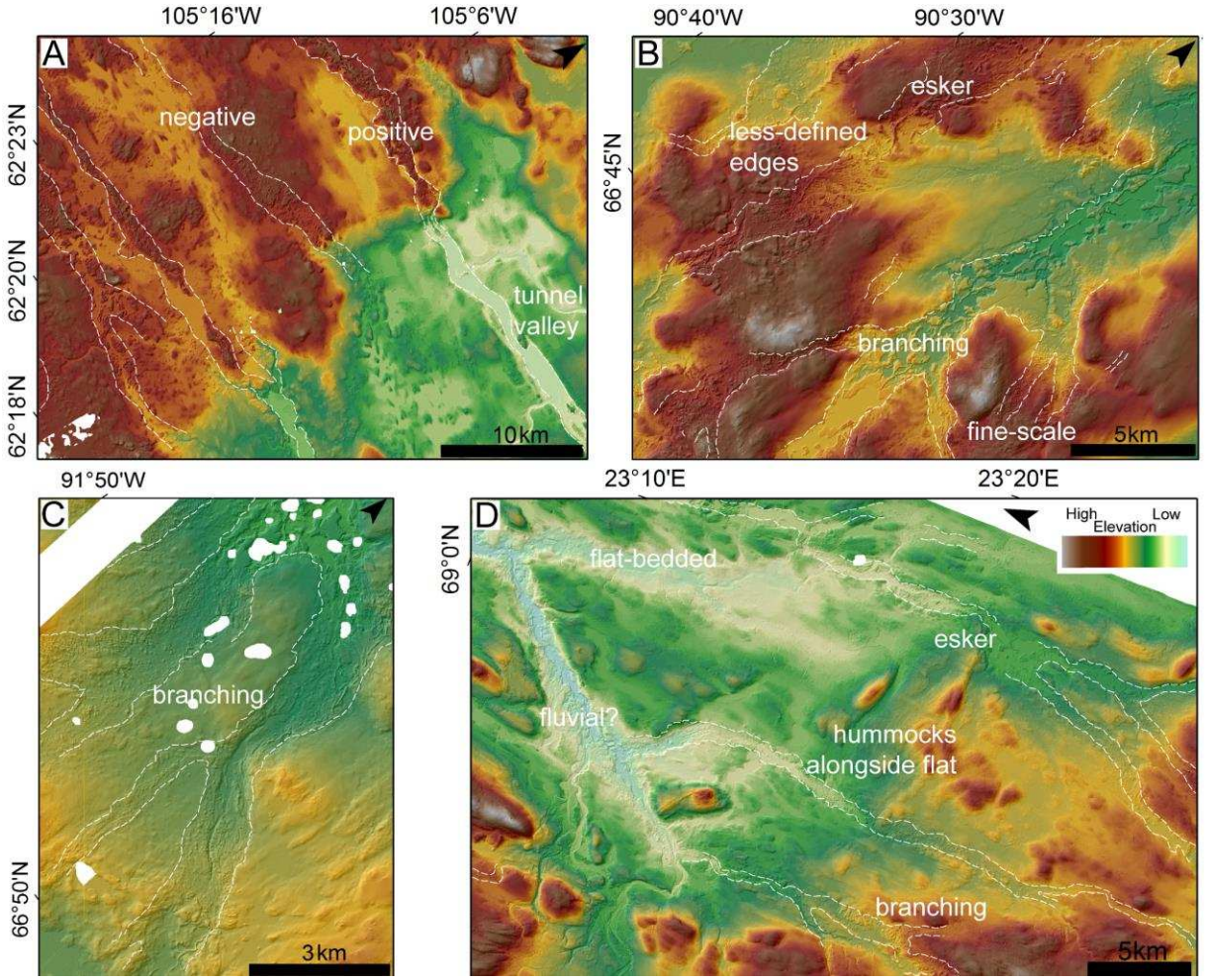

227

228 Figure 5. Example of hummock corridors (outlined in white dashed lines) from each of the
229 test sites with locations identified in Figures 9 -11. (A) Test site 1 - note the transition down-

flow (inferred ice flow from east to west) from tunnel valley to hummock corridor associated with an increase in elevation and the alternating positive and negative hummock corridors. (B and C) Test site 2 – note the more complex hummock corridors that branch and can be difficult to identify on the bed owing to their more subdued relief. (D) Test site 3 – example of hummock corridors branching off a large central channel with few/ no hummocks in places.

3.1 Processing Step One: Filter to isolate hummocks by size

Elevation values in a DEM vary significantly, depending on the presence of large-scale topographic features (e.g. valleys, hills, mountains etc.) and/ or the type of landforms present. Typically, landforms fall within a definable length-scale range. In theory, mathematical operations can be applied to a DEM to isolate a particular feature based on this knowledge. Using length-scales to separate morphological features of interest from background topography is well established within the earth sciences (e.g. Wessel, 1998; Hillier and Watts, 2004; Hillier and Smith, 2008) and has been used within glacial geomorphology to enhance the detection of subtle features such as lineations (Hillier and Smith, 2008).

Individual hummocks from the three test sites were randomly selected, measured (long axis) and recorded to determine their typical length-scale range. To minimise overlap with features which tend to co-occur with hummock corridors, drumlins, eskers and background ‘noise’ in the DEM (artefacts which often occur in elongate patches) were also sampled (their minor axis). The results (Fig. 6) reveal a typical length-scale of 40 - 180 m for hummocks. This is distinguishable from the ‘noise’ and the drumlins at the lower and upper bounds. Although eskers display

255 similar length-scale as hummocks, their low density largely precludes their
256 classification as hummock corridors at later stages of our processing.
257
258 The length-scale range was used to inform the design of a 2D Gaussian-
259 weighted band-pass filter (filt2: written by Chad A. Greene of the University of Texas
260 Institute for Geophysics for use in Matlab - freely available at:
261 https://uk.mathworks.com/matlabcentral/fileexchange/61003-filt2-2d-geospatial-data-
262 filter). The band-pass filter suppresses spatial frequencies outside the specified
263 length-scale range, thus attenuating (although not eliminating) a large amount of the
264 topographic variation associated with other features on the bed. Values of 40 and
265 150 m were selected as the lower and upper bounds as this struck the best balance
266 between retaining information whilst preventing false detections. This resulted in a
267 residual surface with a large amount of background topographies removed,
268 emphasising areas with features within the length-scale of individual hummocks.

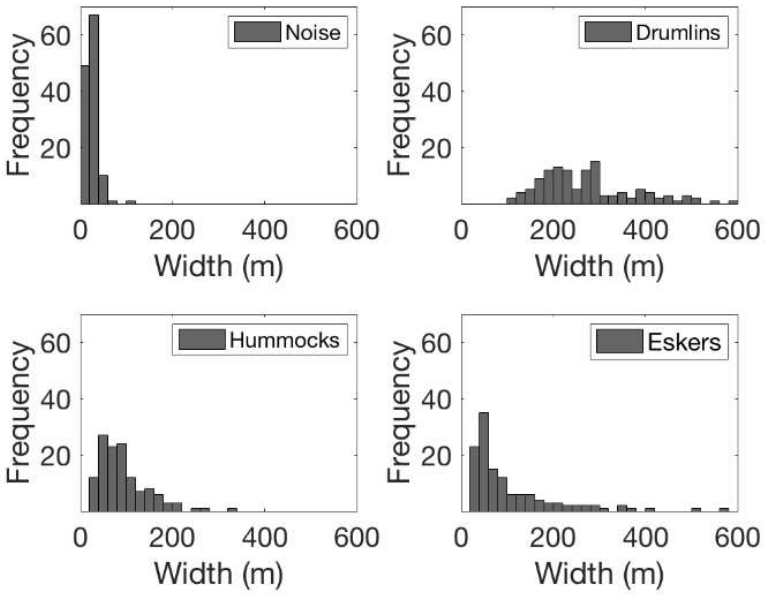

269
270 Figure 6. Histograms showing the horizontal widths of 'noise', drumlins, hummocks and
271 eskers (n = 130) randomly selected and measured from the three test sites. Note that the

hummocks form their own population with only a small overlap at the upper and lower ends. A large amount of the 'noise' (artefacts in the DEM that sometimes occur in linear zones) was smaller than 10 m thus preventing accurate measurement.

For some hydrological features (e.g. lakes and rivers) and in areas of cloud cover or shadows, the ArcticDEM tiles contain no elevation data and were coded as NaN (i.e. Not a Number). While the 2D Gaussian-weighted band-pass filter is designed to work on data with NaNs, several of the subsequent processing steps require continuous data so a method to fill in the NaNs was implemented. Standard interpolation or smoothing methods (e.g. inpaint_nans - https://uk.mathworks.com/matlabcentral/fileexchange/4551-inpaint_nans) can be used to fill NaNs with realistic values over smaller areas; however, the large size of some missing data patches here (up to ~480 km^2) would result in the introduction of artefacts and thus render this approach inappropriate. To address this, we developed a method for 'flooding' isolated NaN patches with their individual local mean. Firstly, a mask of contiguous patches of NaNs was created. The mean elevation of a 100-pixel wide buffer around each patch was then used to replace the NaNs within. This was carried out after the initial filtering, which removed a large amount of elevation variations, creating more uniform values within the NaN buffers and reducing the likelihood of steep jumps in elevation across short distances. While this approach precluded the detection of hummock corridors within these areas, it effectively blended the missing data with its surroundings preventing spurious artefacts. NaN values in the original data were returned to zero at the final stage to ensure that no areas were falsely classified.

297 To further enhance the contrast in relief at the length-scale created by the
298 band-pass filter, the residuals were converted to absolute values and each pixel
299 replaced with the maximum of the adjacent pixels if the original value was greater
300 than the tile median or replaced with the minimum of the adjacent pixels if the
301 original value was less than the median. (This process is analogous to ‘contrast
302 stretching’ in the processing of grey-scaled images.) This ‘enhanced’ residual
303 surface was then normalised by rescaling the data so values fell between 0 and 255
304 (i.e. unsigned 8-bit integers) to ensure consistency between different tiles and to
305 minimise memory requirements for storing data (Fig. 8a).

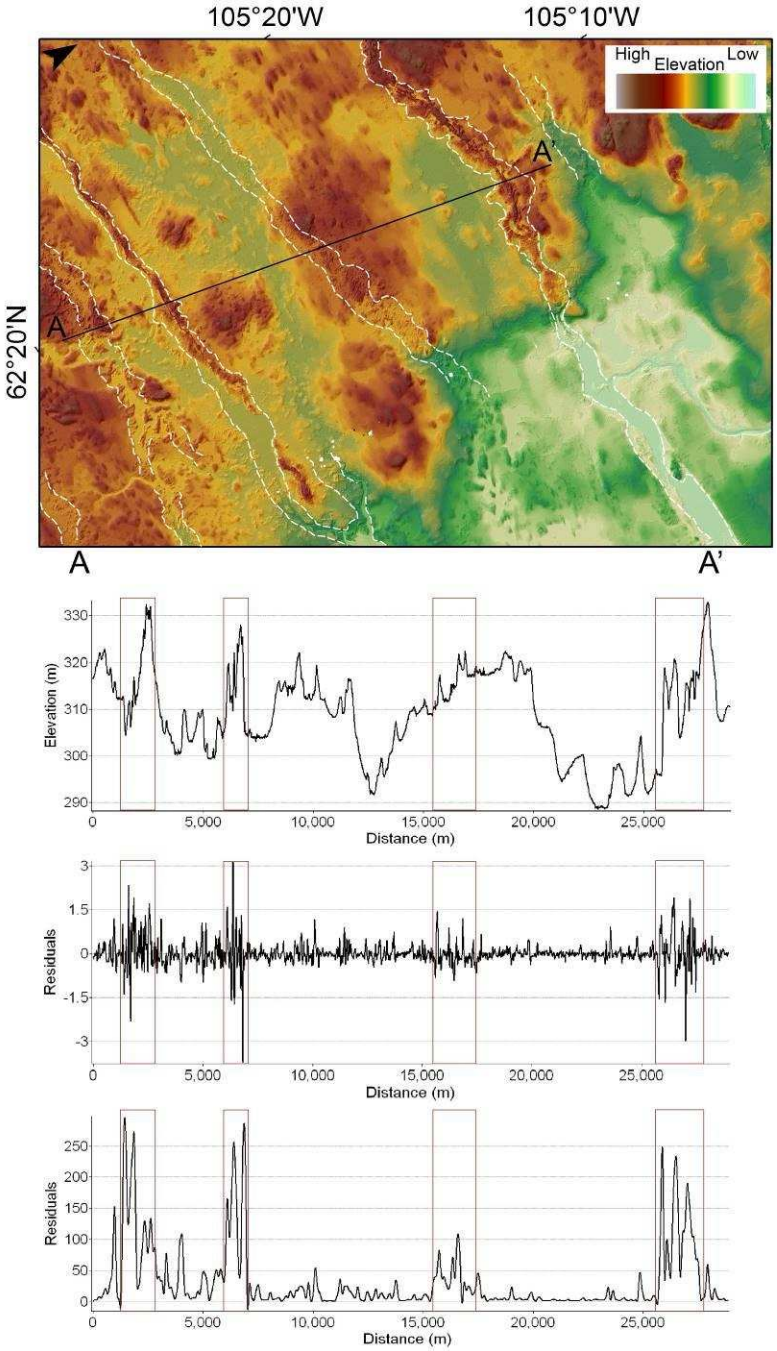

306

307 Figure 7. Cross-profiles across four hummock corridors (red boxes) showing top to bottom:
308 (i) original elevation data with significant elevation variations, (ii) residual surface created
309 post band-pass filter and (ii) residual surface created following enhancement.

310

311

312

313

3.2 Processing Step Two: Filter to remove misaligned features

At regional scales, long axes of hummock corridors are typically observed to have a (sub-) parallel arrangement (e.g. Peterson et al., 2017). We therefore applied a Fast Fourier Transform (FFT) to each enhanced DEM tile to identify the dominant orientation of hummock corridors and remove misaligned features. FFTs are commonly used in image analysis to identify and remove interference or artefacts and to analyse repeating patterns and extract features (e.g. Van Buren, 1987; Tsai and Hsieh, 1999; Jordan and Schott, 2005; Arrell et al., 2008; Munch et al., 2009). In glaciology, FFTs have been used to map crevasses from remotely sensed images (e.g. Williams et al., 2018) and to automatically derive the spectral signature of mega-scale glacial lineations (MSGLs) (Spagnolo et al., 2017).

The FFT produces a power spectrum array of the enhanced DEM in the frequency domain, with the zero-frequency component (measuring the 'average' elevation) located at the centre of the array. In the frequency domain, directional features are identified as a concentration of high-intensity pixels (i.e. bright areas), reaching out from the centre, perpendicular to the direction of the feature in the spatial domain (Fig. 8b). We applied a 'wedge-shaped' filter to the FFT of the enhanced DEM to extract features aligned with the dominant direction of the image, and reject misaligned features. To automate this process and allow the width and orientation of the wedge filter to vary with each input tile, we extracted the highest 2% of the power spectrum, creating a binary mask (Fig. 8c). The shape of this mask varies depending on the 'strength' of the directionality in the image. The amplitude distribution of a tile's FFT (in the 2D frequency domain) generated an ellipse-shaped

mask when there were well-defined hummock corridors while less well-defined/ no corridors resulted in a circular shape. Identifying the start and end points of the long axis of the mask allowed us to use trigonometry to determine its angle relative to the x-axis (tan(x) = change in x / change in y) and this was used as the orientation input for the wedge-filter. Next, we calculated the length of the minor-axis and divided it by three –based on sensitivity analysis – to determine the wedge filter width (i.e. how far it could deviate from the centreline Fig. 8d). Once the filter had been applied and the misaligned features removed, the FFT was inverted to return the filtered data back into the spatial domain (e.g. Fig. 8e).

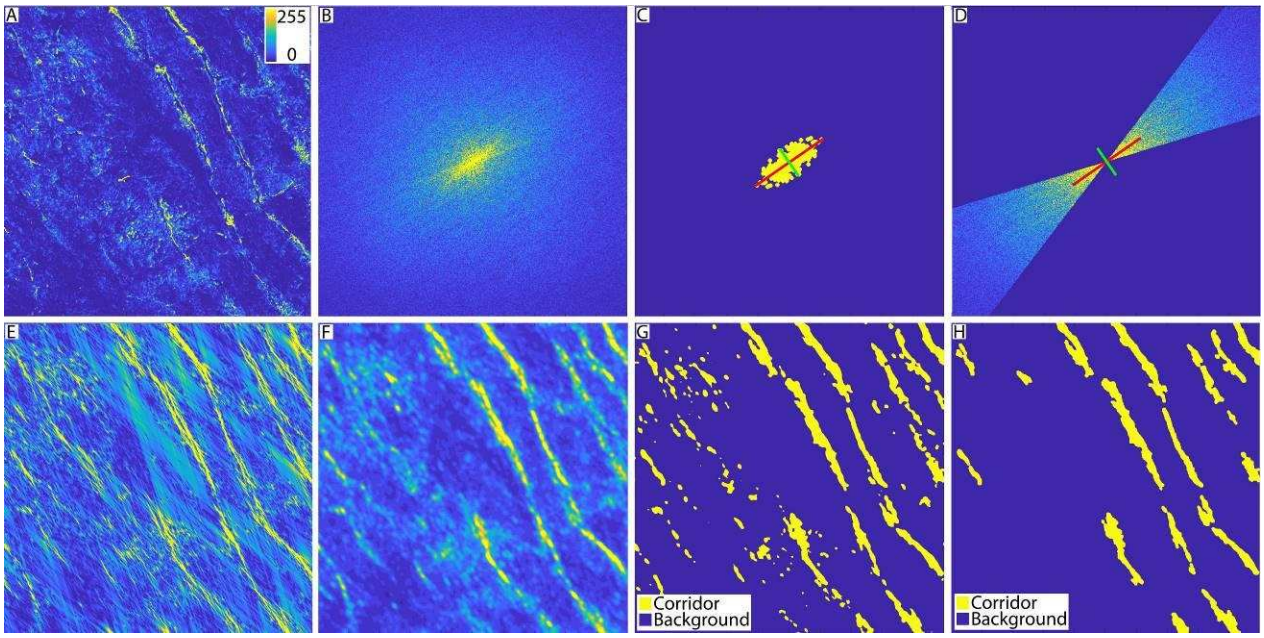

Figure 8. Example of directional filter: (A) DEM tile post-spatial filter and enhancement (but pre FFT filter) with scale bar representing intensity. (B) FFT power spectrum in the frequency domain with the 'average' at the centre and the directional trend evident from the peaks reaching out. (C) FFT mask i.e. highest 2% of the power spectrum with long (red) and short (green) axes identified. (D) 'Wedge' shaped filter overlain on the FFT – inside the wedge information is retained whilst outside (blue) is rejected. (E) Tile post spatial and FFT filtering i.e. data returned to the spatial domain (colour scale limited to intensity of 50 to

356 highlight corridors). (F) Tile post standard deviation and smoothing (colour scale limited to
357 intensity of 20 to highlight corridors). (G) Tile post segmentation. (H) Tile post clean up i.e. a
358 binary image where corridors have a value of 1 (yellow) and the background has a value of 0
359 (blue).
360
361 **3.3 Processing Step Three: Image Segmentation**
362
363 Image segmentation is the final processing stage used to extract hummock
364 corridors. It is commonly used in image processing to divide an image into distinct
365 regions, each containing pixels with similar characteristics e.g. colour or texture (e.g.
366 Haralick and Shapiro, 1985; Ryherd and Woodcock, 1996; Baatz and Schape,
367 2000). Thresholding is the simplest image segmentation technique and produces a
368 binary image with two sections, each containing solely pixels with intensity values
369 either greater or smaller than the threshold. Here, we wished to select a threshold
370 which separates pixels which likely contain hummock corridors (high values) from
371 those which do not (low values). The above steps have been designed to enhance
372 the contrast between these two areas.
373
374 To minimise user input, an automatic method for selecting the threshold was
375 chosen. Here, we used the approach of Otsu (1979) which detects a threshold based
376 on a histogram of pixel intensity values. Otsu's method is optimal when the
377 foreground is distinctly different from the background (e.g. a white object on a black
378 background) and when there is limited intensity variation within each of the two
379 regions. To ensure the best output, we enhanced the difference between hummock
380 corridors and their background further. Standard deviation was used as a measure of
381 topographic roughness, highlighting areas with a high degree of local variations (i.e.

382 ‘rough’ sections of the bed within the hummock corridors where topographic
383 variations had been retained). A 12-by-12 moving average filter was then passed
384 over the residual surface to homogenise the corridors (Fig. 8f).
385
386 The image was then segmented using the threshold determined by the Otsu
387 (1979) method creating a binary image of corridors (with a value of 1) and
388 background (with a value of 0) (Fig. 8g). Next, we applied several post-processing
389 methods to improve the segmentation output (Fig. 8h). To improve the corridors
390 longitudinal completeness, we used a series of morphological operations available in
391 Matlab to bridge gaps (‘bwmorph, bridge’) in the data. We then filled any interior
392 holes (‘imfill, holes’) and smoothed the edges (imopen with a disk structuring
393 element). False classifications were recognisable in the data as small ‘speckles’,
394 objects with low elongation values or objects which did not conform to the dominant
395 orientation. To remove these, we specified several criteria. Firstly, individual objects
396 in the final mask must have (i) an area exceeding 1500 pixels, (ii) an elongation ratio
397 greater than 1.5 (comparison with manual mapping suggests that rough regions with
398 a value less than this are not corridors), and (iii) they must be aligned within +/- 40˚
399 of the dominant direction. The last criterion removed erroneous ‘patches’ since ‘real’
400 misaligned features had already been removed by the FFT.
401
402 **3.4 Accuracy Quantification**
403
404 Finally, to quantify how well the automatic output captured ‘reality’ we
405 undertook an accuracy assessment. Detailed manual mapping of hummock corridors
406 at the three test sites were used as a reference dataset to compare with the

automatic output. Hummock corridors were mapped as polygons to allow for direct comparison with the automatic output through on-screen digitization in ArcGIS 10.4. Hummock corridors were identified as regions of hummocks which stood out from the surrounding smooth, streamlined bed, often exhibiting a positive/ negative relief and association with eskers.

The spatial scale selected for accuracy assessment is important and will likely influence the results (e.g. Dungan, 2002; Stehman and Wickham, 2011). As a first-order measure of accuracy we compared the manual and automatic datasets at the pixel-scale. More detailed analysis at the landform-scale was then performed to assess the methods' utility in reproducing the spatial distribution, pattern and morphology of hummock corridors at an ice-sheet scale. We consider the landform scale accuracy assessment the more appropriate measure for determining the method's ability to provide insight into the formation and evolution of subglacial meltwater pathways.

3.4.1 Pixel-scale

To compare the datasets at a pixel-scale, the manual and automatic output were overlain and each pixel classified as either:

- True Positive (TP) – positive in the reference and automatic output
- False Positive (FP) – negative in the reference and positive in the automatic output
- True Negative (TN) – negative in the reference and automatic output

- False Negative (FN) – positive in the reference and negative in the automatic output

where TP represents the location of pixels classified as hummock corridors, FP represents pixels classified as hummock corridors in the automatic but not in the reference (i.e. over-estimation), TN represents background pixels in both data and FN represents pixels classified as hummock corridors in the manual but not in the automatic (i.e. under-estimation). This information was recorded in an error matrix.

Using this information, we calculated more specific measures of quality:

$$\text{recall} = \frac{\text{TP}}{(\text{TP+FN})} * 100 \qquad \text{(equation 1)}$$

$$\text{precision} = \frac{\text{TP}}{(\text{TP+FP})} * 100 \qquad \text{(equation 2)}$$

where recall indicates how much of the reference data are captured by the automatic output (i.e. 'completeness') and precision indicates how much of the automatic output matches the reference data (i.e. 'correctness'). These measures have been used in remote sensing and OBIA accuracy assessments (e.g. Hillier et al., 2015; Zhang et al., 2015; Pratomo et al., 2017).

3.4.2 Landform-scale

To quantify landform-scale accuracy, we used region-based precision and recall indicators. The approach was similar to the pixel-scale method described in section 3.4.1, but, instead of overlaying and comparing individual pixels, we

compared individual corridors. To achieve this, we first determined our match criteria and mapping direction. A match criteria specifies the minimum overlap required between the manual and automatic mapping before a 'match' is confirmed. This criterion varies in the literature; d'Oleire-Otmanns et al., (2013) consider any overlap a success, Eisank et al., (2014) select a minimum of 50% overlap and Jorge and Brennand (2017) use two criteria (i) a 'morphometric detection rate' requiring a 50% minimum overlap and additional divergence criteria and (ii) a 'general detection rate' requiring a 10% minimum overlap. Here, we select a minimum overlap of 25%. While this is lower than the 50% often used, the size of many of these features is significantly greater than those in the literature above (which is focussed on drumlins) and visual assessment suggests that a minimum 25% match is able to capture the hummock corridors sufficiently.

The mapping direction determines which way we compare the two datasets – i.e. manual to automatic or automatic to manual. This alternates when calculating precision and recall for region-based measures (Zhang et al., 2015). For recall (i.e. 'completeness'), we matched the automatic segments to the reference. Conversely, for precision (i.e. 'correctness'), we matched the reference polygons to the automatic segments. For both recall and precision, corridors which overlapped by greater than the minimum overlap (25%) were classified as true positives, while corridors which were overlapped by less than the minimum overlap or with no overlap, were classified as false positives and false negatives respectively.

3.4.3 Morphology

If we wish to use the output of the automatic method to gain meaningful information about the morphometry of hummock corridors, it is important to assess how well the automatic mapping matches the morphometric characteristics of the manually mapped dataset. Here, we automatically extracted metrics (length and width) for each corridor from both datasets. To obtain the most representative results, pre-processing of the manual and automatic mapping were undertaken to separate corridor networks and individual corridors into discrete features. This was done manually in ArcGIS with care taken to avoid bias in the results by splitting features only where there was obvious evidence of trunk/ tributary corridors, merging (e.g. small pixel bridges), clear change in orientation of features or evidence of elongated sections joining falsely classified ‘patches’. The overall clarity of the output may be further improved by separating the ‘patches’ (i.e. falsely classified sections) from the elongated data (i.e. the hummock corridors) and selectively removing them.

The length of each corridor was calculated automatically by identifying the furthest two boundary pixels and measuring the straight-line distance between them. As hummock corridors can be long, width was measured using perpendicular transects at 5% intervals along each corridor. An average value was then assigned, ensuring that variations in width were captured for all corridors, regardless of their length. Finally, ‘real-length’ was approximated by dividing the area of the hummock corridor by its mean width (henceforth referred to simply as ‘length’).

4. Results

4.1 Automatic method performance

4.1.1 Pixel-scale assessment

[illegible] [illegible]

At test site 1 (Table 2), recall was 45% and precision 33%. This was the highest recall value of the three test sites and likely reflects the fact that test site 1 contains the longest, widest corridors with the most pronounced relief and clear boundary edges. Test site 2 had a 42% recall and 36% precision. This was the highest precision value of the test sites, indicating the lowest percentage of 'false' classifications. At test site 3, recall was 16% and precision 6%, which is significantly lower than the other two sites and visual inspection confirms this is because the automatic method misidentifies several large valleys as hummock corridors.

Table 2. Error matrix showing the number of correctly/ incorrectly identified pixels at each test site. These values were used to calculate further measures of accuracy i.e. precision and recall (equations 1 and 2).

		Automatic: Yes	**Automatic: No**
TS 1	**Manual: Yes**	31001304 (TP)	37947732 (FN)
	Manual: No	62046071 (FP)	1061300000 (TN)
TS2	**Manual: Yes**	46188919 (TP)	63775215 (FN)
	Manual: No	81485389 (FP)	1008300000 (TN)
TS3	**Manual: Yes**	4057104 (TP)	21866102 (FN)
	Manual: No	63649814 (FP)	810426980 (TN)

4.1.2 Landform-scale assessment

4.1.2.1 Region-based recall and precision

The number of corridors correctly/ incorrectly identified at each test site is summarised in table 3. These values were used to produce a measure of precision and accuracy (equations 1 and 2).

Table 3. Error matrix showing the number of correctly/ incorrectly mapped hummock corridors at each test site. Results for both matching directions are included i.e. manual to automatic (for calculating recall) and automatic to manual (for calculating precision) as manual and automatic datasets do not always have the same number of hummock corridors.

		Automatic: Yes	Automatic: No	Total Manual
TS 1 Recall	Manual: Yes	118 (TP)	106 (FN)	224
	Manual: No			
	Total Automatic			
TS 1 Precision	Manual: Yes	108 (TP)		
	Manual: No	115 (FP)		
	Total Automatic	223		
TS 2 Recall	Manual: Yes	194 (TP)	371 (FN)	565
	Manual: No			
	Total Automatic			
TS 2 Precision	Manual: Yes	153 (TP)		
	Manual: No	153 (FP)		
	Total Automatic	306		
TS 3 Recall	Manual: Yes	64 (TP)	105 (FN)	169
	Manual: No			

	Total Automatic		
	Manual: Yes	43 (TP)	
TS 3 Precision	Manual: No	150 (FP)	
	Total Automatic	193	

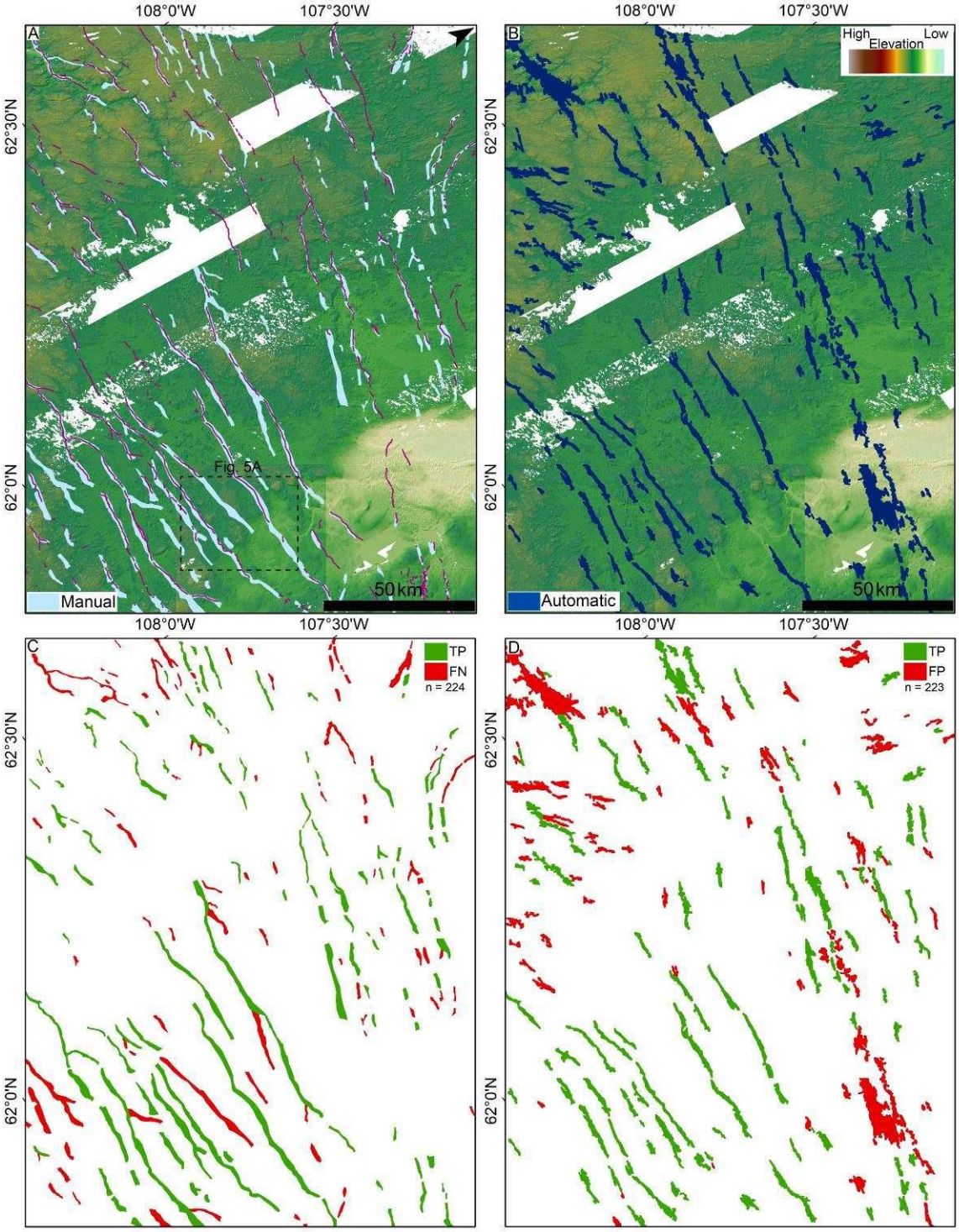

551

552 Figure 9. Large-scale manual (a) and automatic (b) mapping of hummock corridors in test
553 site 1 (near Dubawnt Lake, Canada - former ice-flow from E to W). Manually mapped eskers
554 are also shown in (a) as pink lines. The success of the method is assessed in (c) and (d).
555 Corridors which exhibit a > 25% minimum overlap are coloured green (i.e. True Positives –
556 match in the manual and automatic) while corridors with < 25% minimum overlap are

coloured red. In (c) these are False Negatives (i.e. manual corridors missed) and in (d) False Positives (i.e. incorrectly identified automatic corridors). N = the total number of corridors in each group.

Comparison of the manual and automatic outputs (table 4) indicates a combined recall of 39% and precision of 42%. However, there is considerable inter-test site variation, with site 1 giving the highest recall (53%) and site 2 the lowest (34%). The highest precision is at site 2 (50%) and the lowest at site 3 (22%). In general, the quality of the automatic mapping is improved when compared at the landform scale rather than per pixel, particularly in more complex regions (e.g. site 3 – Fig. 11).

Table 4. Summary of region-based recall and precision measures (equations 1 and 2) by test site using a > 25% minimum overlap criteria.

	Recall (%)	Precision (%)
TS1	53	48
TS2	34	50
TS3	38	22
Combined Results	39	42

Manual and automatic mapping for each test site can be seen in Figures 9, 10 and 11 (a) and (b) respectively. The outcome of the accuracy assessment can be visualised in (c) and (d) with corridors with > 25% overlap coloured green and those with < 25% overlap coloured red.

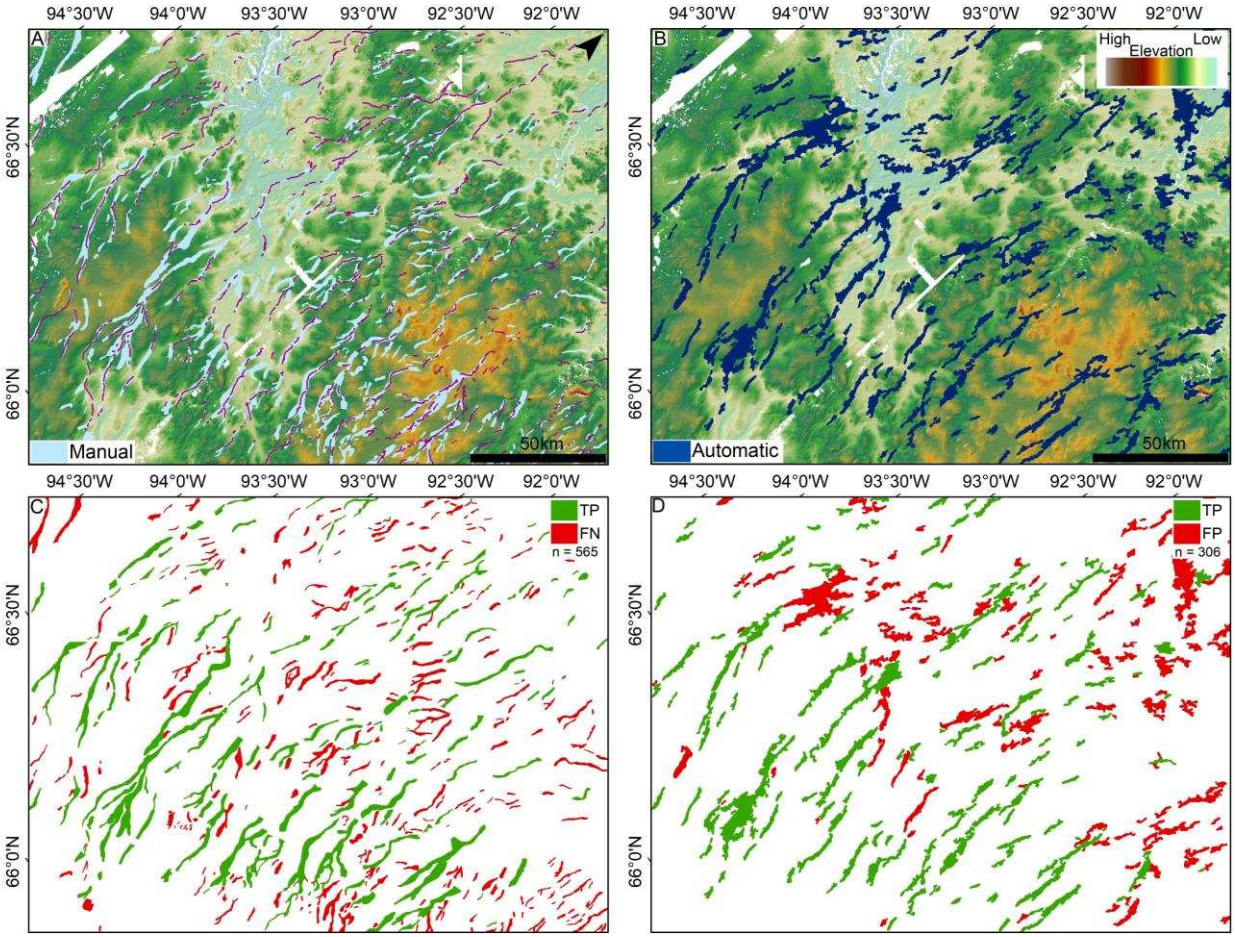

583

584 Figure 10. Large-scale manual (A) and automatic (B) mapping of hummock corridors in test
585 site 2, Nunavut, Canada (former ice-flow from S to N). Manually mapped eskers are also
586 shown in (A) as pink lines. The success of the method is assessed in (C) and (D). Corridors
587 which exhibit a > 25% minimum overlap are coloured green (i.e. True Positives – match in
588 the manual and automatic) while corridors with < 25% minimum overlap are coloured red. In
589 (C) these are False Negatives (i.e. manual corridors missed) and in (D) False Positives (i.e.
590 incorrectly identified automatic corridors). N = the total number of corridors in each group.

591

592 Results indicate that the automatic method can capture corridors of varying
593 morphology, including those with positive and negative relief and branching
594 networks. Automatically detected hummock corridors can be traced over significant
595 distances, even when the features curve across the landscape or cross DEM tile

596 boundaries. However, it is also clear that the corridors missed in the automatic
597 output are often narrower and 'finer-scale' in expression i.e. they have more subdued
598 relief, fewer, more widely distributed or smaller individual hummocks, or they are
599 separated by bounding sections of flat-bed that are unlikely to be detected.

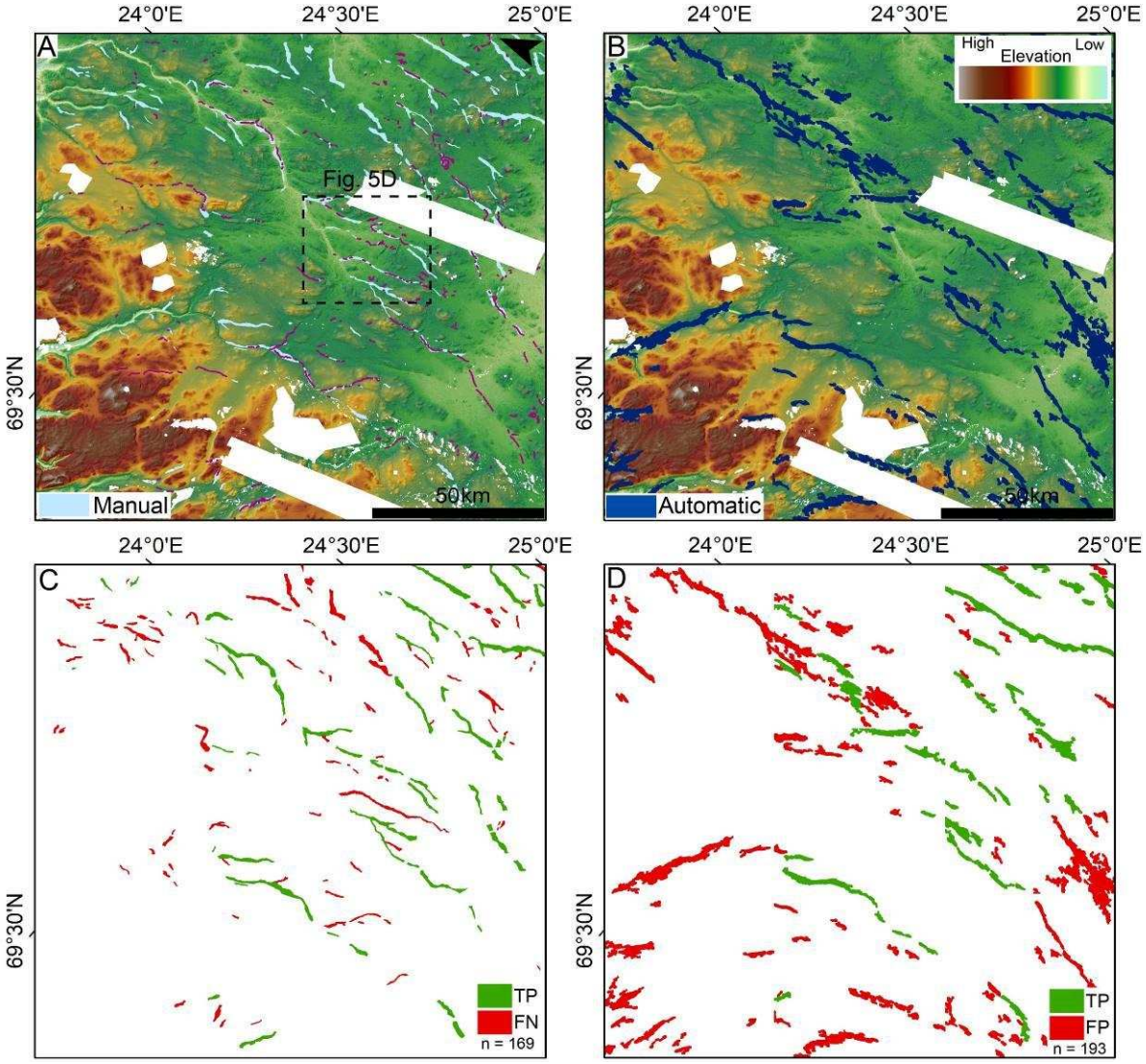

600

601 Figure 11. Large-scale manual (A) and automatic (B) mapping of hummock corridors
602 in test site 3, northern Scandinavia (former ice-flow from S to N). Manually mapped eskers
603 are also shown in (A) as pink lines. The success of the method is assessed in (C) and (D).
604 Corridors which exhibit a > 25% minimum overlap are coloured green (i.e. True Positives –
605 match in the manual and automatic) while corridors with < 25% minimum overlap are

606 coloured red. In (C these are False Negatives (i.e. manual corridors missed) and in (D)
607 False Positives (i.e. incorrectly identified automatic corridors). N = the total number of
608 corridors in each group.
609
610 Given that the automatic method under-detects narrower corridors, we
611 explored whether there was a critical value below which the method was less able/
612 unable to detect features. This was investigated by evaluating the recall value (i.e.
613 percentage of the manually mapped corridors correctly identified) as minimum
614 corridor width was increased (Fig. 12). Corridor detection rate increased from 39%
615 for all corridors to 80% when just corridors wider than 1.4 km were considered.
616 Recall values increased roughly linearly with corridor width at test sites 1 and 2. At
617 test site 3, recall values increased up until ~0.6 km whereupon they started to drop
618 again. This is attributed to the narrower corridors at this site, with only two corridors
619 wider than 1.2 km.

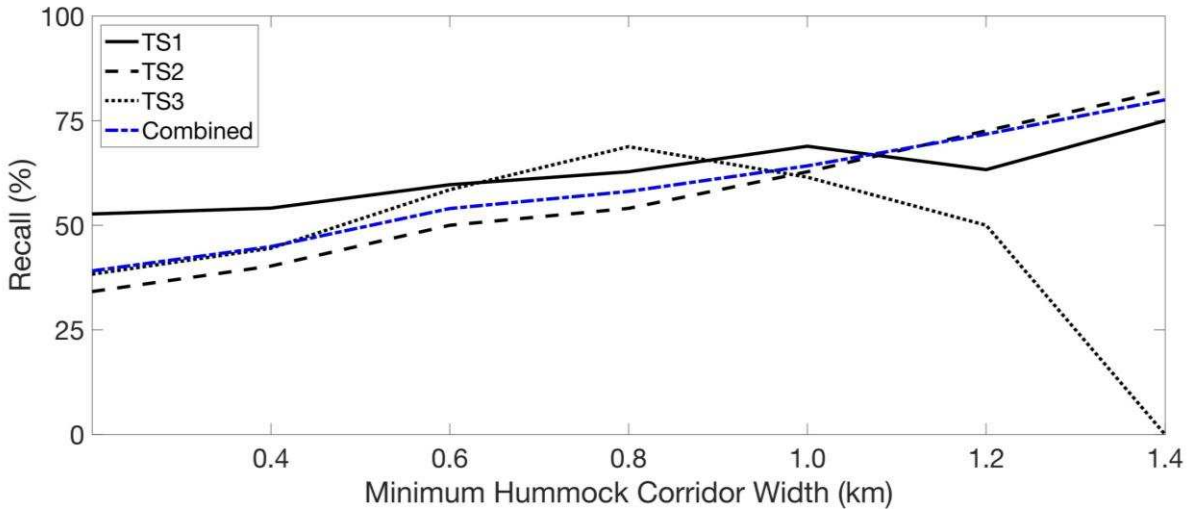

620
621 Figure 12. Change in recall value as minimum width of hummock corridors included in the
622 calculation increases (all to only > 1.4 km).

As the automatic output does a better job at detecting wider corridors, we also calculated the overall area of correctly identified corridors. At test site 1, the corridors identified as true positives account for 69% of the total area of manually mapped corridors. Similarly, the corridors identified as true positives account for 64% and 62% of the total area for test sites 2 and 3 respectively. Therefore, while 50 - 60% of the corridors are missed by the automatic approach (Table 4), the corridors that match represent a higher proportion of the overall area. This suggests that the automatic method is capable of approximating the large-scale distribution and pattern of hummock corridors, even though some of the finer-scale detail is lost.

4.1.2.2 Morphology

The length and width of hummock corridors in the manual and automatic outputs are first compared by investigating their frequency distributions (Fig. 13) and descriptive statistics (Table 5). The manual mapping and automatic mapping display similarity in these distributions, including a positive skew indicating a high abundance of shorter (less than 10 km) and narrower (less than 2 km) hummock corridor segments. In general, the mean and median are similar, particularly for the combined data set (~ 1,000 corridor segments for all 3 sites) and for corridor length.

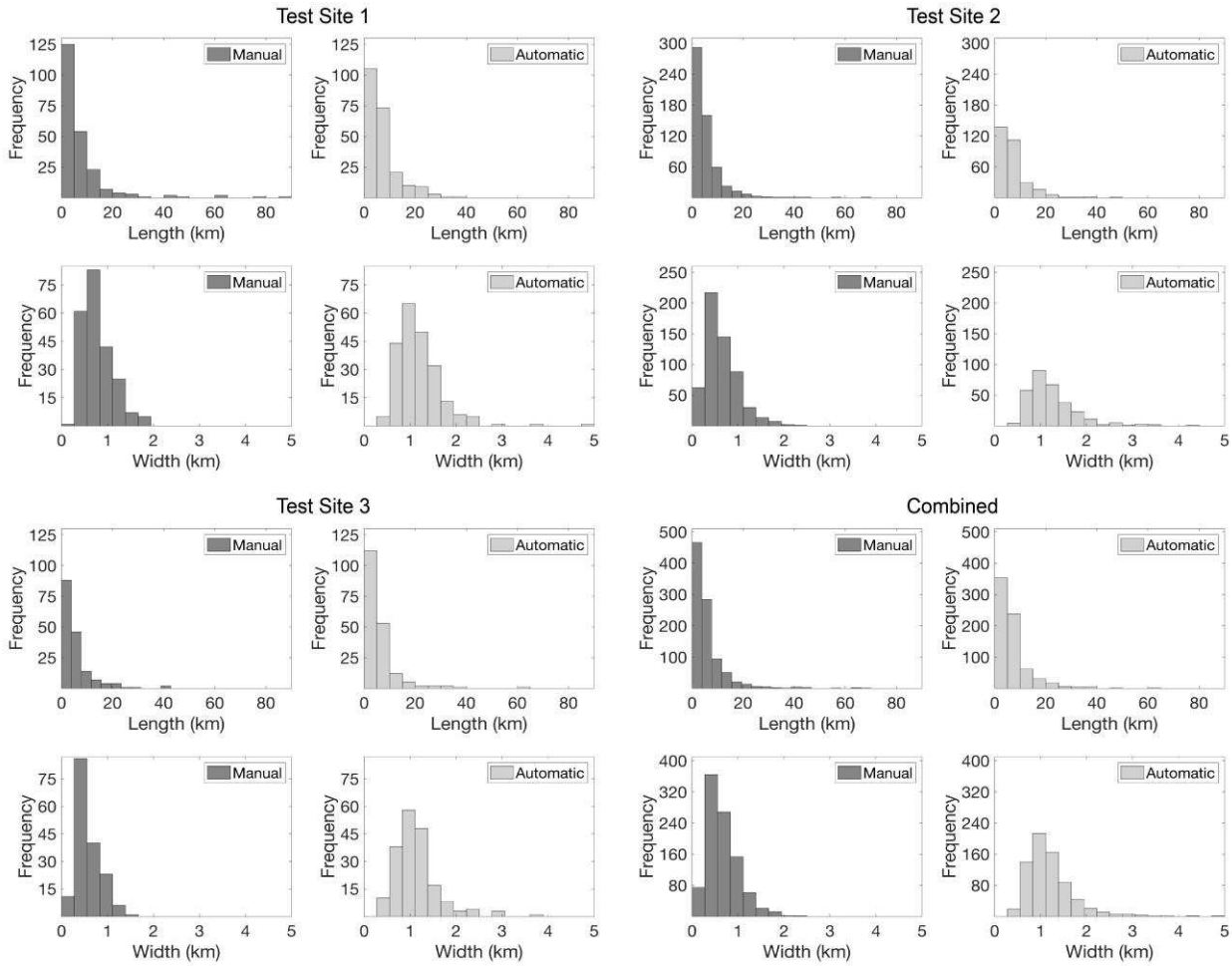

649

650 Figure 13. Frequency distribution of automatic and manually mapped hummock corridor
651 real- length and width for each test site. (Width bins of 5 km for length and 0.2 km for width.)

652

653 Nonetheless, there are also some differences between the manual and
654 automatic metrics; noticeably, a lack of data in the narrowest width bins in the
655 automatic output, which helps explain the overall higher mean and median widths of
656 hummock corridors at each test site (Table 5). In section 4.1.2.1, above, we
657 demonstrate that this systematic under-estimation occurs because the automatic
658 method struggles to identify narrower corridors.

659

The automatic output fails to capture the longest manually mapped segments as is shown by significantly lower maximum lengths (Table 5). However, in general the mean and median values for manual and automatic lengths are much closer than the widths (only varying by 0.7 km and 0.5 km for the combined dataset: n = 958 for the manual corridors and n = 722 for the automatic). This suggests that the automatic method does a better job at capturing length than width. A Wilcoxon Rank Sum Test (equivalent to Mann-Whitney U-Test) was used to test the similarity of the automatic and manual measurements at each test site. The null hypothesis (i.e. that the automatic and manual measurements were from distributions with the same median) was rejected at the 5% significance level for all comparisons, excluding the automatic and manual lengths at test site 1 (p-value = 0.2056).

Table 5. Descriptive statistics for manual and automatic mapping (length and width (km)) for each test site and combined across all three.

		Test Site 1		**Test Site 2**		**Test Site 3**		**Combined**	
		Length (km)	Width (km)	Length (km)	Width (km)	Length (km)	Width (km)	Length (km)	Width (km)
Mean	manual	8.1	0.8	5.7	0.6	5.7	0.6	6.3	0.7
	automatic	7.4	1.2	7.1	1.2	6.4	1.1	7.0	1.2
Median	manual	4.6	0.7	3.8	0.6	3.7	0.5	4.0	0.6
	automatic	5.4	1.1	5.3	1.1	4.2	1.1	5.0	1.1
Standard Dev.	manual	11.3	0.3	6.3	0.4	6.2	0.3	7.8	0.3
	automatic	6.2	0.5	6.0	0.5	7.0	0.5	6.3	0.5
Min	manual	1.1	0.2	0.7	0.1	0.8	0.0	0.7	0.0
	automatic	1.1	0.5	1.2	0.5	1.1	0.5	1.1	0.5
Max	manual	90.0	1.9	69.0	2.5	39.2	1.6	90.0	2.5
	automatic	35.9	4.9	46.4	4.4	61.3	3.9	61.3	4.9

5. Discussion

5.1 Overall performance

Our approach has facilitated the identification and mapping of almost 1,000 hummock corridor segments across 82,500 km^2, largely reproducing their overall distribution (i.e. successfully capturing 69%, 64% and 62% of their total area at each test site) and morphometry compared to manual mapping (i.e. largely reproducing the length/ width distributions). The output of this study provides insight into the expression and variation of these features, and contributes to an increasing body of literature on them (e.g. St-Onge, 1984; Rampton, 2000; Utting et al., 2009; Sharpe et al., 2017; Peterson and Johnson, 2018).

The output of the automatic method has created a near-continuous map of hummock corridors which aligns hummock corridor segments across adjacent ArcticDEM tile boundaries and is able to recreate the general pattern across a large area. While some of the finer detail is lost, this method nevertheless has value for rapidly (< 80 seconds per 50 x 50 km^2 5m resolution tile, run on the University of Sheffield High Performance Computer cluster – Iceberg – with a specified memory of 32 GB) assessing significant volumes of data and providing information on hummock corridor distribution and spatial arrangement and extracting information on morphometry. Furthermore, assessing many hummock corridors across significant areas makes it more likely that we will capture a more representative dataset and allows us to assess their association with other bed features.

5.2 Limitations

5.2.1 Hummock corridor morphology

Despite progress in the automatic detection and mapping of subglacial bedforms, several limitations exist which need to be acknowledged before assessing and using the output. The automatic method fails to identify all the manually mapped hummock corridors across the three test sites. While this does not appear to influence our understanding of the general location nor the large-scale trends of hummock corridors (i.e. general direction, length and width) or their association with other bedforms, it does suggest that some detail is being lost.

Further exploration of the reasons for this suggests that hummock corridor morphology influences whether they are detected and retained in the final output. The automatic output is sensitive to hummock corridor width, with detection rates increasing as corridor width increases (from 39% when all corridors are included to 64% for corridors wider than 1 km and up to 80% for corridors greater than 1.4 km). It is likely that narrower corridors are removed during the filtering stages or when the data resolution is reduced and the results smoothed. Many of the wider corridors are also longer and this highlights issues related to the discontinuous nature of hummock corridors. Hummock corridor segments detected automatically likely represent parts of a larger corridor/ network of corridors, fragmented because of 'real' gaps in the corridor (e.g. areas of flat bed or areas with too few hummocks to be detected/ retained) or because of the side-effects of processing prior to metric extraction (i.e. separating trunk/ tributary corridors). This means that they should be

taken as a minimum hummock corridor length and should we choose to interpolate between segments, it is likely that the hummock corridors would reach greater lengths and form more complete networks. Assessing the automatic map of hummock corridors without interpolating between the segments, means that we are unlikely to capture the full length of the manual mapping as a single, complete feature. The gaps along flow may be a possible reason for not detecting more complete corridors despite increased widths.

5.2.2 Background conditions

As hummock corridor morphology cannot fully explain why corridors were/ were not detected, we must also consider other possible causes for imperfect detection (rates below 100%). One such consideration is differences in surface roughness across the bed. Hummock corridors display variations in expression (e.g. relief, definition, hummock density) both within and across sites and this makes it difficult to develop a method which can automatically detect all of them whilst also minimising false classifications. Despite our best efforts to filter out the background, confounding roughness elements are sometimes retained. Large sections of the bed surrounding test site 3 in northern Scandinavia have greater variation in relief than those in Canada and there is more likely to be evidence of human activities. These areas of confounding roughness may be classified as hummock corridors regardless of their possible lack of exposure to subglacial meltwater flow, especially if they exhibit characteristics comparable with the pre-defined criteria for hummock corridors. Similarly, other background features such as fluvial channels and geologically controlled landforms may also be classified as hummock corridors. This

753 is a particular problem when these features have a ‘stronger’ directional trend than
754 any hummock corridors in the same tile skewing the FFT wedge filter and thus
755 inadvertently removing hummock corridors. It is possible that these features are part
756 of the same subglacial hydrological network (e.g. Fig. 5D); however, if they are not,
757 inclusion of additional steps such as overlying the automatic output on the DEM/
758 geology map would allow the user to manually identify erroneous areas (often by
759 shape and size) and assess case by case whether these should be deleted or
760 retained.
761
762 **5.2.3 Manual mapping and Accuracy Quantification Methods**
763
764 It is important to acknowledge the subjectivity and limitations of manually
765 mapping hummock corridors in general, especially those on complex backgrounds or
766 those which form part of a larger glaciofluvial complex where boundaries are unlikely
767 to be discrete. Some of the hummock corridors observed across the study sites are
768 less pronounced in terms of their overall relief and/ or the relief/ number of the
769 hummocks within them making them difficult to manually map. It is therefore unlikely
770 that the automatic method will be able to capture these either given that the filtering
771 and coarsening steps remove some detail. It is also likely that individual manual
772 mappers would map these differently. As such, manual mapping is not necessarily
773 ‘true’ nor should we expect the automatic method to reproduce it perfectly.
774
775 Furthermore, instead of just missing corridors, there are examples from the test
776 sites where the automatic method can differentiate hummock corridors from complex
777 backgrounds, even identifying some which were missed/ incompletely mapped by

778 the manual mapping. Ultimately, the automatic method relies on pre-defined
779 decision-making criteria which determine the eventual mapping of corridors. This
780 means that the results are consistent, repeatable and defensible (Saha et al., 2011).
781
782 Finally, we must also consider how we interpret the accuracy measures when
783 determining how well the automatic output fits the reference data. While it is useful
784 for providing a quantitative summary of how many corridors are detected at each
785 site, it does not consider additional factors which are relevant here. For example,
786 individual inspection of corridor segments suggests that in some cases, using a
787 minimum of 25% meant that some 'real' corridors were incorrectly missed.
788 Furthermore, the method gives equal weighting to every corridor, regardless of its
789 size.
790
791 **5.3 Future work**
792
793 **5.3.1 Methodological developments**
794
795 Depending on the desired use and output of this method, several steps can be
796 undertaken to enhance the results, should they be required. For example, mapping
797 can be compared to geological maps, maps of water bodies and maps of other
798 subglacial bedforms (e.g. rogen moraines, tunnel valleys etc.) which may have been
799 misclassified as hummock corridors by the automatic method. Furthermore, visually
800 assessing the output in a GIS software will draw the eye to areas which are
801 particularly 'blocky' in nature and which clearly stand out. The user can then make
802 their own decision as to whether this information should be removed.

803 Visual assessment of the results suggests that misidentification is typically
804 associated with narrower features or additional features on the bed exhibiting strong
805 directional trends, such as fluvial channels in test site 3, or in some cases linear
806 tracts of drumlins. Future work may reduce the influence of this for example, by
807 trialling the code on different resolution data or by using different sized sample tiles.
808 Determining the scale at which the hummock corridors remain aligned may allow the
809 user to alter the input tile size as a way of reducing the likelihood of additional
810 directional features influencing the FFT filter.
811
812 **5.3.2 Applications**
813
814 Within the test sites, there is a clear association between hummock corridors and
815 other subglacial meltwater landforms. For example, at test site 1, the down-flow
816 transition from tunnel valleys to hummock corridors coincides with an increase in
817 elevation of approximately 30 m (Fig. 5A). At test sites 1 and 2 there is a striking
818 similarity in the overall pattern and distribution of eskers (Storrar et al., 2014) and
819 hummock corridors (Fig. 9 - 11). By running the automatic method over a large
820 section of northern Canada, we will be able to compare the general distribution and
821 pattern to that of eskers at an ice-sheet scale. The output of this can be used to
822 guide more detailed manual mapping, significantly reducing mapping time by
823 drawing the eye to areas of interest, after which the manual mapper can ‘fill in the
824 gaps’. While this method is yet to be tested on other features, theoretically it should
825 be possible to use our approach to identify other bedforms which share a predefined
826 horizontal size range and orientation. For example, it may be possible to alter the
827 parameters slightly and use this to map eskers or drumlins.

6. Conclusions

This work has been motivated by the large-scale release of high resolution ArcticDEM data which allows subglacial bedforms to be mapped at an unprecedented spatial and temporal scale. Hummock corridors have been widely identified on the beds of palaeo-ice sheets, and the results of our automated mapping method offer the potential to rapidly gain a large amount of information on the morphological characteristics and large-scale distribution of hummock corridors. This will add to the existing literature and can be used to inform the development of hypotheses for hummock corridor formation.

Given the increasing availability of high-resolution data, there is a need to develop new methods which can rapidly obtain meaningful information directly from DEMs. While automatic mapping may never reach the same level of detail and precision as manual mapping for individual bedforms, it has potential when the main aim is to quantify the large-scale pattern of landforms. In this study, we add to an increasing body of literature on the development of automatic methods for the identification and mapping of palaeo-subglacial bedforms by developing the first automatic method for extracting spatial information on hummock corridors. We apply this method to three test sites across the ArcticDEM and demonstrate that hummock corridors with varying expressions and varying background conditions can be identified. Results suggest that our method can capture the general location and spatial pattern/ distribution of hummock corridors and provides a decent ‘first pass’ map which can later be refined manually depending on the desired output.

For this study, the ability to correctly identify each hummock is less important than the method's ability to capture the location and overall pattern of corridors and when considering a large sample size, the results (i.e. Table 5 – combined sites) suggest that the automatic method can accurately characterise their morphology. The next step will be to use this method to map hummock corridors using the ArcticDEM data for Canada and northern Scandinavia, thus gaining unprecedented insight into the large-scale distribution and pattern of hummock corridors and their association with other subglacial bedforms and meltwater features. This will provide evidence for formation theories as well as information which can be used to better understand the distribution and nature of subglacial meltwater flow beneath former and current ice-sheets.

7. Acknowledgements

This work was funded through "Adapting to the Challenges of a Changing Environment" (ACCE); a NERC funded doctoral training partnership ACCE DTP (NE/L002450/1). DEMs provided by the Polar Geospatial Centre under NSF-OPP awards 1043681, 1559691, and 1542736. We would like to thank Sarah Greenwood and Kang Yang for useful discussions. We would also like to thank Mike Smith, Andrew Finlayson and the editor for their reviews that resulted in significant improvements to the manuscript.

8. Data availability

The numerical code developed in this paper is archived at: https://doi.org/10.15131/shef.data.7999445.

9. References

Anderson, R.S. et al., 2004. Strong feedbacks between hydrology and sliding of a small alpine glacier. Journal of Geophysical Research. 109(F3).

Andrews, L.C. Catania, G.A. Hoffman, M.J. Gulley, J.D. Luthi, M.P. Ryser, C. Hawley, R.L. Neumann, T.A. 2014. Direct observations of evolving subglacial drainage beneath the Greenland Ice Sheet. Nature. 514(7520): 80-3.

Arrell, K. Wise, S. Wood, J. Donoghue, D. (2008). Spectral filtering as a method of visualising and removing striped artefacts in digital elevation data. Earth Processes and Landforms. 33(6): 943-61.

Baatz, M. Schäpe, A. (2000) Multiresolution Segmentation: An Optimization Approach for High Quality Multi-Scale Image Segmentation. In: Strobl, J., Blaschke, T. and Griesbner, G., Eds., Angewandte Geographische Informations-Verarbeitung, XII, Wichmann Verlag, Karlsruhe, Germany, 12-23.

902 Bartholomew, I. Nienow, P. Mair, D. Hubbard, A. King, M.A. Sole, A. 2010. Seasonal
903 evolution of subglacial drainage and acceleration in Greenland outlet glacier.
904 Nature Geoscience. 3: 408-11.
905
906 Bishop, M.P. Allan James, L. Shroder, J.F. Walsh, S.J. (2012). Geospatial
907 technologies and digital geomorphological mapping: Concepts, issues and
908 research. Geomorphology. 137: 5-26.

909 Boulton, G.S. Clark, C.D. (1990). A highly mobile Laurentide Ice Sheet revealed by
910 satellite images of glacial lineations. Nature. 346: 813-17.

911 Boulton, G.S. Dobbie, K.E. Zatsepin, S. 2001. Sediment deformation beneath
912 glaciers and its coupling to the subglacial hydraulic system. Quaternary
913 International. 86: 3-28.
914
915 Burke, M.J. Brennand, T.A. Perkins, A.J. (2011). Erosional corridor evolution in
916 south-central British Columbia: insights from ground-penetrating radar
917 surveys. Proceedings of Geohydro 2011.
918
919 Chandler, D.M. Wadham, J.L. Lis, G.P. Cowton, T. Sole, A. Bartholomew, I. Telling,
920 J. Nienow, P. Bagshaw, E.B. Mair, D. Vinen, S. Hubbard, A. 2013. Evolution
921 of the subglacial drainage system beneath the Greenland Ice Sheet revealed
922 by tracers. Nature Geoscience. 6.

923 Clark, C.D. Evans, D.J.A. Khatwa, A. Bradwell, T. Jordan, C.J. Marsh, S.H. Mitchell,
924 W.A. Bateman, M.D. (2004). Map and GIS database of glacial landforms and
925 features related to the British Ice Sheet. Boreas. 33: 359-75.

926 Clark, C.D. Hughes, A.L.C. Greenwood, S.L. Jordan, C. Sejrup, H.P. (2012). Pattern
927 and timing of retreat of the last British-Irish Ice Sheet. Quaternary Science
928 Reviews. 44: 112-46.

929 Clark, C.D. Livingstone, S.J. (2018). Glacial curvilineations found along the southern
930 sector of the Laurentide Ice sheet and a hypothesis of formation involving
931 subglacial slope failure in tunnel valleys and subglacial lakes. Earth Surface
932 Processes and landforms. 43(7): 1518-1528.

933 Clark, P.U. Walder, J.S. (1994). Subglacial drainage, eskers and deforming beds
934 beneath the Laurentide and Eurasian ice sheets. Geol. Soc. Am. Bull. 106:
935 304-14.

936 d'Oleire-Oltmanns, S. Eisank, C. Dragut, L. Blaschke, T. (2013). An object-based
937 workflow to extract landforms at multiple scales from two distinct data types.
938 IEEE Geoscience and Remote Sensing Letters. 10(4): 947-51.

939 Dungan, J.L. (2002). Toward a comprehensive view of uncertainty in remote sensing
940 analysis. In Uncertainty in Remote Sensing and GIS, G.M. Foody and P.M.
941 Atkinson (Eds). Pp 25-35. (Chichester, UK: Wiley).

942 Dyke, A.S. Prest, V.K. (1987). Late Wisconsinan and Holocene history of the
943 Laurentide ice sheet. Geog. Phys. Quat. 41: 237-64.

944 Eisank, C. Smith, M.J. Hillier, J.K. (2014). Assessment of multiresolution
945 segmentation for delimiting drumlins in digital elevation models.
946 Geomorphology. 214: 452-64.

947 Evans, D.J.A. Clark, C.D. Mitchell, W.A. (2005). The last British Ice Sheet: a review
948 of the evidence utilised in the compilation of the Glacial Map of Britain. Earth
949 Science Reviews. 70: 253-312.

950 Evans, I.S. (2012). Geomorphometry and landform mapping: what is a landform?
951 Geomorphology. 137: 94-106.

952 Foroutan, M. Zimbelman, J.R. (2017). Semi-automatic mapping of linear-trending
953 bedforms using 'Self-Organising Maps' algorithm. Geomorphology. 293(A):
954 156-66.

955 Greenwood, S.L. Clark, C.D. (2008). Subglacial bedforms of the Irish Ice Sheet.
956 Journal of Maps. 4(1): 325-57.

957 Greenwood, S.L. Clark, C.D. Hughes, A. (2007). Formalising an inversion
958 methodology for reconstructing ice-sheet retreat patterns from meltwater
959 channels: application to the British Ice Sheet. Journal of Quaternary Science.
960 22: 637-45.

961 Haralick, R. Shapiro, L. (1985). Image segmentation techniques. Computer Vision,
962 Graphics, and Image Processing. 29: 100-32.

963 Hillier, J.K. Smith, M. (2008). Residual relief separation: digital elevation model
964 enhancement for geomorphological mapping. Earth Surface Processes and
965 Landforms. 33: 2266-76.

966 Hillier, J.K. Smith, M. Armugam, R. Barr, I. Boston, CM. Clark, C.D. Ely, J. Fankl, A.
967 Greenwood, S.L. Gosselin, L. Hättestrand, C. Hogan, K. Hughes, A.L.C.
968 Livingstone, S.J. Lovell, H. McHenry, M. Muñoz, Y. Pellicer, X.M. Pellitero, R.

969 Robb, C. Roberson, S. Ruther, D. Spagnolo, M. Standell, M. Stokes, C.R.
970 Storrar, R. Tate, N.J. Wooldridge, K. (2015). Manual mapping of drumlins in
971 synthetic landscapes to assess operator effectiveness. Journal of Maps.
972 11(5): 719-29.

973 Hillier, J.K. Watts, A.B. (2004). “Plate-like” subsidence of the East Pacific Rise-South
974 Pacific superswell system. Geomagnetism and Paleomagnetism/ Marine
975 Geology and Geophysics. 109(B10).

976 Hughes, A. Clark, C.D. Jordan, C. (2010). Subglacial bedforms of the last British ice
977 sheet. Journal of Maps. 543-63.

978 Iken, A. 1981. The effect of subglacial water pressure on the sliding velocity of a
979 glacier in an idealized numerical model. Journal of Glaciology. 27 (97): 407-
980 21.
981
982 Jordan, G. Schott, B. (2005). Application of wavelet analysis to the study of spatial
983 pattern of morphotectonic lineaments in digital terrain models. A case study.
984 Remote Sensing of Environment. 94: 31-38.
985
986 Jorge, M.G. Brennand, T.A. (2017). Semi-automated extraction of longitudinal
987 subglacial bedforms from digital terrain models – Two new methods.
988 Geomorphology. 288: 148-63.

989 Kleman, J. (1992). The palimpsest glacial landscape in north-west Sweden.
990 Geografiska. 74A: 306-25.

991 Kleman, J. Borgstrom, I. (1996). Reconstruction of palaeo-ice sheets: the use of
992 geomorphological data. Earth Surface Processes and Landforms. 21: 893-
993 909.

994 Kleman, J. Glasser, N.F. (2007). The subglacial thermal organisation (STO) of ice
995 sheets. Quaternary Science Reviews. 26(5-6): 585-97.

996 Livingstone, S.J. Clark, C.D. (2016). Morphological properties of tunnel valleys of the
997 southern sector of the Laurentide Ice Sheet and implications for their
998 formation. Earth Surface Dynamics. 4: 567-89.

999 Livingstone, S.J. Utting, D.J. Ruffell, A. Clark, C.D. Pawley, S. Atkinson, N. Fowler,
1000 A.C. (2016). Discovery of relict subglacial lakes and their geometry and
1001 mechanism of drainage. Nature Communications. 7. 11767.

1002 Makinen, J. Kajuutti, K. Palmu, J.-P. Ojala, A. Ahokangas, E. (2017). Triangular-
1003 shaped landforms reveal subglacial drainage routes in SW Finland.
1004 Quaternary Science Reviews. 164: 37-53.

1005 Margold, M. Jansson, K.N. Kleman, J. Stroeven, A.P. Clague, J.J. (2013). Retreat
1006 pattern of the Cordilleran Ice Sheet in central British Columbia at the end of
1007 the last glaciation reconstructed from glacial meltwater landforms. Boreas. 42:
1008 830-47.

1009 Margold, M. Stokes, C.R. Clark, C.D. (2015). Ice streams in the Laurentide Ice
1010 Sheet: Identification, characteristics and comparison to modern ice sheets.
1011 Earth Science Reviews. 143: 117-46.

1012 Munch, B. Trtik, P. Marone, F. Stampanoni, M. (2009). Stripe and ring artefact
1013 removal with combined wavelet – Fourier filtering. Optic Express. 17(10):
1014 8567-91.

1015 Noh, M-J. Howat, I.M. (2015). Automated stereo-photogrammetric DEM generation
1016 at high latitudes: Surface Extraction with TIN-based Search-space
1017 Minimization (SETSM) validation and demonstration over glaciated regions.
1018 GIScience and Remote Sensing. 52(2): 198-217.

1019 Ó Cofaigh, C., Stokes, C.R. (2008). Reconstructing ice-sheet dynamics from
1020 subglacial sediments and landforms: introduction and overview. Earth Surface
1021 Processes and Landforms 33(4): 495-502.

1022 Otsu, N. (1979). A threshold selection method from gray-level histograms. IEEE
1023 Transactions on Systems, Man, and Cybernetics. SMC-9.

1024 Ottesen, D. Stokes, C.R. Rise, L. Olsen, L. (2008). Quaternary ice-sheet dynamics
1025 and ice streaming along the coastal parts of northern Norway. Quaternary
1026 Science Reviews. 27: 19.

1027 Peterson, G. Johnson, M.D. Colby, A. Smith. (2017). Glacial geomorphology of the
1028 south Swedish uplands – focus on the spatial distribution of hummock tracts.
1029 Journal of Maps. 13(2): 534-44.

1030 Peterson, G. Johnson, M.D. Dahlgren, S. Passe, T. Alexanderson, H. (2018).
1031 Genesis of hummocks found in tunnel valleys: an example from Hörda,
1032 southern Sweden. GFF. 140(2): 189-201.

1033 Peterson, G. Johnson, M.D. (2018). Hummock corridors in the south-central sector
1034 of the Fennoscandian ice sheet, morphometry and pattern. Earth Surface
1035 Processes and Landforms. 43: 919-29.

1036 Pratomo, J. Kuffer, M. Martinez, J. Kohli, D. (2017). Coupling uncertainties with
1037 accuracy assessment in object-based slum detection case study: Jakarta,
1038 Indonesia. Remote Sensing. 9(11).

1039 Rampton, V.N. (2000). Large-scale effects of subglacial meltwater flow in the
1040 southern Slave Province, Northwest Territories, Canada. Canadian Journal of
1041 Earth Sciences. 37(1): 81–93.
1042
1043 Ryherd, S. Woodcock, C.E. (1996). Combining spectral and texture data in the
1044 segmentation of remotely sensed images .Photogrammetric Wngineering and
1045 Remote Sensing. 62(2): 181-94.
1046
1047 Saha, K. Wells, N.A. Munro-Stasiuk, M. (2011). An object-orientated approach to
1048 automated landform mapping: A case study of drumlins. Computers and
1049 Geosciences. 37(9): 1324-36.
1050
1051 Schoof, C., 2010. Ice-sheet acceleration driven by melt supply variability. Nature.
1052 468(7325): 803–6.
1053
1054 Sharp, M. Gemmel, J. Tison, J. (1989). Structure and stability of the former
1055 subglacial drainage system of the Glacier de Tsanfleuron, Switzerland. Earth
1056 Surface Processes and Landforms. 14(2): 119-134.

Sharpe, D. Kjarsgaard, B. Knight, R.D. Russell, H.A.J. Kerr, D.E. (2017). Glacial dispersal and flow history, East Arm area of Great Slave Lake, NWT, Canada. Quaternary Science Reviews. 165: 49-72.

Sjogren, D.B. Fisher, T.G. Taylor, L.D. Jol, H.M. Munro-Stasiuk, M.J. 2002. Incipient tunnel channels. Quaternary International. 90: 41-56.

Smith, M.J. Clark, C.D. (2005). Methods for the visualisation of digital elevation models for landform mapping. Earth Surface Processes and Landforms. 30(7): 885-900.

Spagnolo, M. Bartholomaus, T.C. Clark, C.D. Stokes, C.R. Atkinson, N. Dowdeswell, J.A. Ely, J.C. Graham, A.G.C. Hogan, K.A. King, E.C. Larter, R.D. Livingstone, S.J. Pritchard, H.D. (2017). The periodic topography of ice stream beds: Insights from the Fourier spectra of mega-scale glacial lineations. Journal of Geophysical Research: Earth Surface. 122(7): 1355-1373.

Stehman, S.V. Wickham, J.D. (2011). Pixels, blocks of pixels, and polygons: Choosing a spatial unit for thematic accuracy assessment. Remote Sensing of the Environment. 115(12): 3044-55.

Stokes, C.R. Clark, C.D. (1999). Geomorphological criteria for identifying Pleistocene ice streams. Annals of Glaciology. 28: 67-74.

1080 Stokes, C.R. et al., (2015). On the reconstruction of palaeo-ice sheets: Recent
1081 advances and future challenges. Quaternary Science Reviews. 125: 15-49.

1082 St-Onge, 1984. Surficial deposits of the Redrock Lake area, District of Mackenzie; in
1083 Current Research, Part A, Geological Survey of Canada, Paper 84 (1A): 271-
1084 78.
1085
1086 Storrar, R.D. Livingstone, S.J. (2017). Glacial geomorhology of the northern Kivalliq
1087 region, Nunavut, Canada, with an emphasis on meltwater drainage systems.
1088 Journal of Maps. 13(2): 153-64.

1089 Storrar, R.D. Stokes, C.R. Evans, D.J.A. (2014). Increased channelisation of
1090 subglacial drainage during deglaciation of the Laurentide Ice Sheet. Geology.
1091 42(3): 239-42.

1092 Storrar, R.D. Stokes, C.R. Evans, D.J.A. (2014). Morphometry and pattern of a large
1093 sample (>20,000) of Canadian eskers and implications for subglacial drainage
1094 beneath ice sheets. Quaternary Science Reviews. 105: 1-25.

1095 Tedstone, A.J. Nienow, P.W. Gourmelon, N. Dehecq, A. Goldberg, D. Hanna, E.
1096 2015. Decadal slowdown of a land-terminating sector of the Greenland Ice
1097 Sheet despite warming. Nature. 526: 692-695.

1098 Tsai, D.M. Hsieh, C.Y. (1999). Automated surface inspection for directional textures.
1099 Image and Vision Computing. 18:49-62.

1100 Utting, D.J., Ward, B.C. & Little, E.C. (2009). Genesis of hummocks in glaciofluvial
1101 corridors near the Keewatin Ice Divide, Canada. Boreas. 38(3): 471–481.

Van Buren, D. (1987). Fourier removal of stripe artefacts in IRAS images. Astronomical Journal. 94: 1092- 94.

Van der Vegt, P. Janszen, A. Moscariello, A. (2012). Tunnel Valleys: current knowledge and future perspectives. In: Husse, M. Reddfern, J. Le Heron, D.P. Dixon, R.J. Moscariello, A. Craig, J. (Eds), Glaciogenic Reservoirs and Hydrocarbon Systems. Geological Society Special Publication, vol. 368: 75-97.

Wessel, P. (1998). An empirical method for optimal robust regional-residual separation of geophysical data. Journal of Mathematical Geology. 30(4): 391-408.

Williams, C. O'Leary, M. Luckman, A. Jóhannesson, T. Murray, T. (2018). Automated crevasse mapping: assisting with mountain and glacier hazard assessment. Geophysical Research Abstracts. Vol. 20. EGU2018-5137.

Wright, H.E. (1973). Tunnel valleys, glacial surges and subglacial hydrology of the Superior Lobe, Minnesota. In: Black, R.F. Goldthwait, R.P. and Willman, H.B. (eds.) The Wisconsian Stage. Geological Society of America, Memoir. 136: 251-76.

Yu, P. Eyles, N. Sookhan, S. (2015). Automated drumlin shape and volume estimation using high resolution LiDAR imagery (Curvature Based Relief Separation): A test from the Wadena Drumlin Field, Minnesota. Geomorphology. 246: 589-601.

Zhang, X. Feng, X. Xiao, P. He, G. Zhu, L. (2015). Segmentation quality evaluation using region-based precision and recall measures for remote sensing. ISPRS Journal of Photogrammetry and Remote Sensing. 102: 73-84.